12-2013

The Effects of Gantry Tilt on Breast Dose and Image Noise in Cardiac CT

Michael Hoppe
Marquette University

Diksha Gandhi
Marquette University

Grant Stevens
GE Healthcare

Dennis Foley
Medical College of Wisconsin

Taly Gilat-Schmidt
Marquette University, tal.gilat-schmidt@marquette.edu

Medical Physics, Vol. 40, No. 12 (December 2013): 121905. DOI.

The Effects of Gantry Tilt on Breast Dose and Image Noise in Cardiac CT

Michael E. Hoppe
Department of Biomedical Engineering, Marquette University, Milwaukee, Wisconsin
Diksha Gandhi
Department of Biomedical Engineering, Marquette University, Milwaukee, Wisconsin
Grant M. Stevens
GE Healthcare, Waukesha, Wisconsin
W. Dennis Foley
Department of Radiology, Medical College of Wisconsin, Froedtert Memorial Lutheran Hospital, Milwaukee, Wisconsin
Taly Gilat Schmidt
Department of Biomedical Engineering, Marquette University, Milwaukee, Wisconsin

Abstract

Purpose:

This study investigated the effects of tilted-gantry acquisition on image noise and glandular breast dose in females during cardiac computed tomography (CT) scans. Reducing the dose to glandular breast tissue is important due to its high radiosensitivity and limited diagnostic significance in cardiac CT scans.

Methods:

Tilted-gantry acquisition was investigated through computer simulations and experimental measurements. Upon IRB approval, eight voxelized phantoms were constructed from previously acquired cardiac CT datasets. Monte Carlo simulations quantified the dose deposited in glandular breast tissue over a range of tilt angles. The effects of tilted-gantry acquisition on breast dose were measured on a clinical CT scanner (CT750HD, GE Healthcare) using an anthropomorphic phantom with MOSFET dosimeters in the breast regions. In both simulations and experiments, scans were performed at gantry tilt angles of 0°–30°, in 5° increments. The percent change in breast dose was calculated relative to the nontilted scan for all tilt angles. The percent change in noise standard deviation due to gantry tilt was calculated in all reconstructed simulated and experimental images.

Results:

Tilting the gantry reduced the breast dose in all simulated and experimental phantoms, with generally greater dose reduction at increased gantry tilts. For example, at 30° gantry tilt, the dosimeters located in the superior, middle, and inferior breast regions measured dose reductions of 74%, 61%, and 9%, respectively. The simulations estimated 0%–30% total breast dose reduction across the eight phantoms and range of tilt angles. However, tilted-gantry acquisition also increased the noise standard deviation in the simulated phantoms by 2%–50% due to increased pathlength through the iodine-filled heart. The experimental phantom, which did not contain iodine in the blood, demonstrated decreased breast dose and decreased noise at all gantry tilt angles.

Conclusions:

Tilting the gantry reduced the dose to the breast, while also increasing noise standard deviation. Overall, the noise increase outweighed the dose reduction for the eight voxelized phantoms, suggesting that tilted gantry acquisition may not be beneficial for reducing breast dose while maintaining image quality.

I. INTRODUCTION

Computed tomography (CT) is the largest source of exposure to ionizing radiation in medicine, contributing approximately 30% of the radiation dose to the population in the United States.[1,2] In 2010, an estimated 80×10^6 CT scans were performed, with the use of CT increasing.[1,3] Due to the increasing role CT serves in patient care, radiation dose mitigation techniques have received greater attention and implementation. One factor contributing to dose concerns is the exposure of diagnostically irrelevant, radiosensitive tissue to ionizing radiation. Such is the case with coronary CT angiography (cCTA) scans which expose radiosensitive glandular breast tissue and lung tissue to ionizing radiation even though they are not the primary organ or tissue of interest.

Due to the exposure of radiosensitive tissues during a standard cCTA scan, there exists an increase in the risk of cancer incidence for patients. The exposure during retrospectively gated cCTA results in an estimated lifetime attributable risk (LAR) for cancer of 1 in 143 for a 20-year old woman, 1 in 284 for a 40-year-old woman, and 1 in 466 for a 60-year old woman. In comparison, the male LAR is 1 in 686 for a 20-year-old man, 1 in 1007 for a 40 year-old man, and 1 in 1911 for a 60-year-old man.[4] In females, the LAR is approximately five times greater at all ages, with the combination of lung and breast cancers contributing 80%–85% (~40% each) of this

risk.[4] Prospective gating reduces the LAR to 1 in 4329 for a 62-year old man and 1 in 4629 for a 62-year-old woman, with the breast receiving the highest weighted equivalent dose in women.[5]

A variety of techniques have been developed to mitigate the risk of cardiac CT scans, for example, prospective ECG gating, ECG-gated tube current modulation with retrospective gating, minimization of the craniocaudal scan length, and optimization of the tube current and voltage.[6–11] To further reduce the risk to women, specific methods to reduce breast dose have also been proposed, including bismuth shields, angular tube current modulation, and partial scanning techniques.[7,12–16] These methods, though effective, may have tradeoffs such as increased image noise in the case of shields and increased spine dose in the case of partial scanning techniques.[7,15,16]

A previous study proposed reducing breast dose by tilting the CT gantry and/or patient so that the beam is parallel to the long axis of the heart.[11] This long-axis acquisition protocol would provide direct acquisition of short-axis cardiac images, and allow the reconstruction of long-axis cardiac images after reformatting. In a retrospective analysis of reconstructed images, the previous study estimated a greater than 50% reduction in breast volume irradiation. However, breast dose and image quality were not quantified.[11] The study also estimated that the tilt angles required to image along the long axis of the left ventricle ranged from 7° to 54°, with the majority between 20° and 40°.[11] Current scanners are limited both by mechanical and physical limitation to a maximum tilt.[11] For example, the clinical system used in this study can tilt up to 30° off the axial plane.

We hypothesize that tilted-gantry acquisition will reduce breast dose, but may incur a noise penalty due to increased pathlengths for rays tilted off of the axial plane. This study estimated radiation dose to glandular breast tissue and reconstructed image noise for commercially available tilt angles of 5°–30° compared to a 0° tilt through simulations and phantom experiments. The energy deposited in the glandular breast tissue and reconstructed image noise standard deviation were estimated using Monte Carlo and ray-tracing simulations with voxelized phantoms (created from CT datasets of eight female patients) and analysis of experimental data collected using one anthropomorphic physical phantom and a clinical scanner.

II. METHODS AND MATERIALS

II.A. Anthropomorphic phantom experiments

Experiments were performed on a clinical CT system (Discovery CT750HD, GE Healthcare, Chalfont St Giles, England) using a standard chest CT protocol (120 kVp, 250 mAs, 1.25 mm slice thickness, step-and-shoot axial scans). Acquisitions were performed with the anthropomorphic Lungman phantom (Kyoto Kagaku Company, Kyoto, Japan) which contains a well-defined “cardiac tissue” volume and detailed lung anatomy but does not model uptake of iodinated contrast agent. To simulate a female patient, three slabs of breast models were taken from the female Rando Phantom (The Phantom Laboratory, Salem, NY) and attached to the Lungman phantom (Fig. **1**). Although using three slabs resulted in an unrealistic flat anterior breast surface (Fig. **2**), this arrangement of slabs was found to more closely model the breast distribution of a supine subject than using the complete rigid breast phantom. To quantify dose to regions of the breast, MOSFET dosimeters (mobileMOSFET Dosimetry System, Best Medical, Ottawa, Canada) were placed in three regions of the breast (superior, intermediate, and inferior) as can be seen in Fig. **1**. The MOSFETs were experimentally verified to be linear in the CT operating range and then calibrated in air and in a CTDI phantom against ionization chamber measurements. The phantom was placed in the scanner bore as shown in Fig. **2** and five acquisitions performed at each gantry tilt angle of 0°–30° in 5° increments. Using the scout images as references, the table was translated after gantry tilt to ensure coverage of the complete heart volume. The experimental CT images were automatically reformatted by the scanner and reconstructed onto 1.25-mm-thick axial slices of 0.8789 × 0.8789-mm pixels.

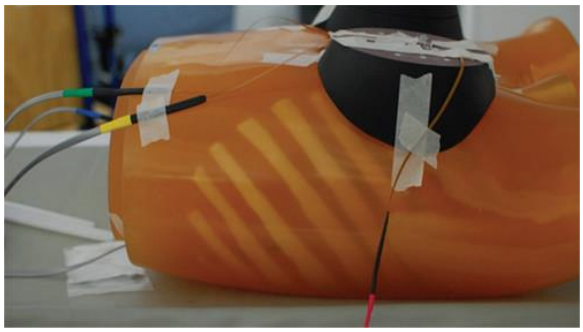

Figure 1 Lungman with RANDO phantom breast models and MOSFET dosimeters.

Figure 2 The GE CT750HD with its gantry tilted to perform a tilted acquisition.

The dose recorded by each dosimeter was averaged across five trials for each tilt angle. The percent change in dose of the tilted acquisition was calculated relative to the 0° tilt for each dosimeter, as expressed in Eq. (1)

$$\%\ \text{change} = 100\left(\frac{\text{dose}_{\text{tilt}}}{\text{dose}_0} - 1\right). \quad (1)$$

The standard deviation was calculated in manually selected volumes of interest (VOIs) in the myocardium of the reconstructed images. The percent change in noise standard deviation of the tilted acquisition relative to the nontilted acquisition was calculated for all phantoms and tilt angles.

II.B. Simulation studies

II.B.1. Simulated CT system specifications

The simulations modeled the experimental CT system with a source-to-isocenter distance of 54 cm, an isocenter-to-detector distance of 41 cm, and a multirow detector with dimensions 3.5 cm (slice direction) × 105 cm (inplane) and pixel dimensions of 0.9765 × 0.9765 mm. A 120 kVp point source with 6.0 mm of Aluminum-equivalent filtration was modeled using the SPEC78 software.[17,18] The 6-mm-Aluminum filtered beam represented the spectrum at the center of the beam, and a beam-shaping filter was also modeled based on specifications available in the literature.[17,19] Step-and-shoot axial acquisitions covering the heart from the aortic arch to the apex were simulated for tilt angles of 0°–30° in 5° increments. Figure **3** depicts the acquired volume thickness on a simulated lateral scout. The number of gantry rotations required to image the volume decreased with increasing tilt angle, as the heart can be imaged using a reduced scan length (i.e., tighter beam) when viewed off the axial plane. As in the experiments, the phantom was repositioned after gantry tilt to maintain the field of view (FOV) in the slice direction.

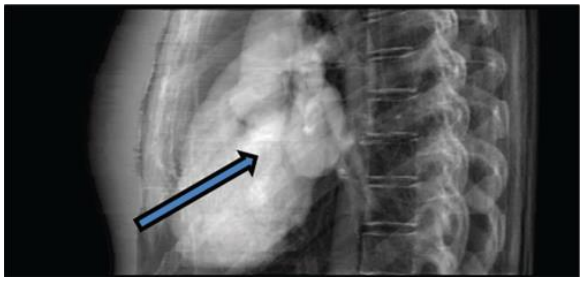

Figure 3 Simulated lateral scout of one voxelized phantom, demonstrating the acquired volume thickness. The arrow represents the projection direction for a 30° gantry tilt.

II.B.2. Simulation methods

Monte Carlo simulations to quantify radiation dose were performed with voxelized phantoms and GEANT4.[20] The voxelized phantoms are described in more detail in Sec. **II B 4**. For all Monte Carlo simulations, the point source transmitted 1.5×10^5 x-ray photons onto the detector surface for each gantry rotation. Each photon and its secondaries were tracked until exiting the simulation's boundaries or until the particle's energy was below the threshold of travelling 0.5 mm, in which case the energy was absorbed. As the photons travelled through the phantom during a simulation, energy deposited in eV per material/tissue was tallied. A total of 360 views (1°/view) were simulated in the Monte Carlo simulations. This number of views was selected to estimate organ dose deposition, which is expected to vary slowly with angle, while reducing the computational requirements of the Monte Carlo simulations. While the number of x-ray photons per view is not representative of realistic output, it was chosen to provide a low variance after consecutive runs of the same simulation. This is admissible as the purpose of this study is to calculate a percent reduction in dose and not to estimate absolute dose values.

To determine the net impact of tilted-gantry acquisition on image noise, ray tracing simulations were performed with and without noise for the voxelized phantoms and modeled CT scanner. The purpose of the study was to quantify relative differences in noise standard deviation with varying tilt angle, rather than quantifying absolute image noise. Therefore, the simulated photon fluence did not necessarily match the output of the experimental system. The polyenergetic spectrum and Poisson distribution of quantum noise were modeled assuming 739 219 photons incident per detector pixel [i.e., a source fluence of 2.97×10^6 photons/mAs mm^2 at 95 cm from the source as determined by SPEC78 (Ref. **18**)] for each of 1000 views (0.36°/view). Images perpendicular to the axis of rotation were reconstructed from the log-normalized sinograms using an inhouse filtered backprojection algorithm with a Hanning-windowed ramp filter. Thus, the angle of the reconstructed images relative to the axial

plane was equal to the tilt angle of the gantry. Images were reconstructed onto 11 slices with voxels of size 0.5 × 0.5 × 0.5 mm centered about the central slice of the heart in order to calculate noise standard deviation in a volume of interest near the central plane of the heart.

II.B.3. Validation of simulation methods with experimental results

The simulation methods were validated by comparing the experimentally measured changes in dose and noise standard deviation across tilt angle with values estimated by simulations. For this validation, a voxelized software model of the experimental anthropomorphic phantom was created by segmenting the reconstructed phantom images into regions of air, water, soft tissue, and bone based on CT number. The MOSFETs were manually segmented by DG. The energy deposited in the MOSFET regions was calculated using the Monte Carlo simulation methods described in Sec. **II B 2** for tilt angles ranging from 0° to 30° in 5° increments. The percent change in dose relative to the 0° tilt was calculated and compared to the experimental results. Ray tracing simulations and image reconstruction was performed as described in Sec. **II B 2**. Noise-only images were generated from the simulated data by subtracting noise-free reconstructed images from noisy images. In the experiments, the reconstructed volume was reformatted by the scanner software to axial slices for all acquired gantry tilt angles. This reformatting typically involves interpolation and may reduce noise for tilt angles greater than zero (at the expense of spatial resolution). In order to validate the simulation methods, the volume reconstructed from simulations was also reformatted onto axial slices using cubic interpolation. After reformatting, the standard deviation was calculated in a VOI in the myocardium region of the noise only images. The percent change in noise standard deviation of the tilted acquisition relative to the nontilted acquisition was calculated for all tilt angles and compared to the experimental results.

II.B.4. Patient-based voxelized phantoms

To quantify the dose and noise standard deviation of tilted-gantry acquisitions for more realistic representations of patient anatomy, simulations were performed using voxelized phantom models created from eight patient datasets. With IRB approval, eight, randomly selected, contrast-enhanced cardiac CT datasets of adult, female subjects were obtained from Froedtert Hospital for the creation of voxelized phantoms. The subject perimeter, as measured on the central slice of the reconstructed cardiac volume by DG, is listed in Table **I** for all subjects.

Table I. Perimeter of the eight voxelized phantoms as estimated on the central axial slice of the cardiac volume.

	S1	**S2**	**S3**	**S4**	**S5**	**S6**	**S7**	**S8**
Perimeter (mm)	793	999	857	975	931	924	901	1089

The datasets contained DICOM images with slice thicknesses of 0.625 mm, and pixel spacing between 0.547 and 0.703 mm. The datasets were semiautomatically segmented into seven materials (adipose, air, blood, bone, glandular breast, lung, and muscle), based on Hounsfield number and location, to create voxelized phantoms as shown in Fig. **4**. Glandular breast tissue was manually segmented in all datasets by MEH. Material compositions were taken from the International Commission on Radiological Protection Publication 110.[21] Blood was modeled as a mixture of iodine and water (iodine concentration of 0.28 g/cm^3), which provided reconstructed HU values similar to those in the contrast-filled heart regions of the original CT datasets. Two of the phantom datasets were cropped in the slice direction, preventing the simulation of tilt angles greater than 20°. These phantoms were included in the study for tilt angles ranging from 0° to 20°. In the simulations, water slabs were placed inferior and superior to the voxelized phantom in order to simulate the effects of scatter outside of the irradiated field of view.

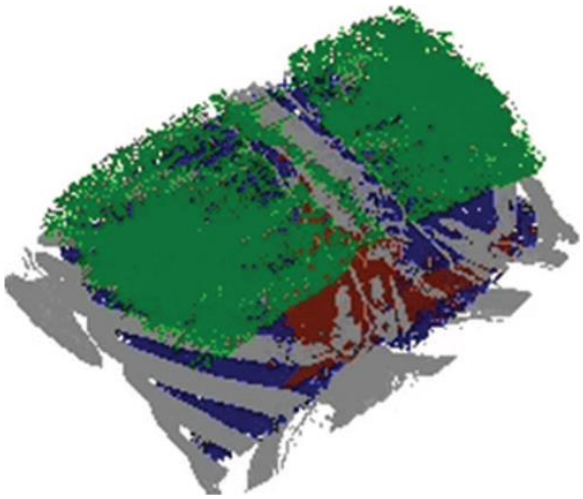

Figure 4 Voxelized phantom including glandular breast tissue, bone, lung, and blood.

The breast size and position varied across voxelized phantom models. The thickness of glandular breast tissue in the anterior-posterior (AP) direction was calculated for each slice of each voxelized phantom. Figure **5** plots the average glandular tissue thickness versus slice number for each voxelized phantom, with slice number zero corresponding to the most superior slice in the volume, whose location varied across the phantoms. The slice thickness for all phantoms was 0.625 mm.

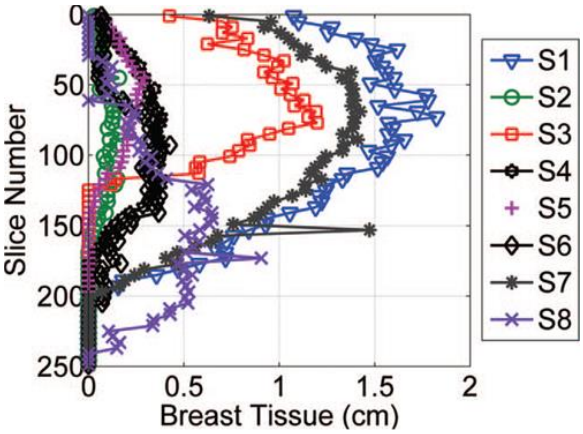

Figure 5 Average thickness of glandular breast tissue at each slice of the eight voxelized phantoms. Each marker corresponds to one voxelized phantom. Slice number zero corresponds to the most superior slice in the phantom.

In the simulation studies, the total energy deposited in the glandular breast tissue was tallied for each phantom. At 0° and 30° tilt, the Monte Carlo simulations were repeated three times to characterize the uncertainty in the deposited energy. At 0° and 30°, the mean, μ, standard deviation, σ, and percent coefficient of variation (COV), %COV = 100%*σ/μ, were calculated for the glandular breast doses across the three trials per tilt angle. Only simulations at a 0° tilt and 30° tilt were run three times due to the assumption that a 0° tilt and a 30° tilt represent the extrema for dose reduction. One simulation was performed for each voxelized phantom at tilt angles between 0° and 30°.

To determine the effects of gantry tilt on image noise, noise-only images were generated from the simulated data by subtracting noise-free reconstructed images from noisy images. Images of the simulated voxelized phantoms were reconstructed onto tilted slices (perpendicular to the tilted axis of rotation) and were not

reformatted onto axial slices. In each simulated dataset, the standard deviation was calculated in a VOI in the noise only image, manually selected within the myocardium. The percent change in noise standard deviation of the tilted acquisition relative to the nontilted acquisition was calculated for all phantoms and tilt angles.

III. RESULTS

III.A. Experimental results and validation of simulation methods

Figure **6** plots the percent change in dose for all studied gantry tilt angles relative to the 0° tilt for dosimeters in the breast regions of the experimental anthropomorphic phantom. Figure **6** also plots the percent change in dose estimated by Monte Carlo simulations of the experimental setup. The largest dose reduction occurred in the superior region of the breast, with a 54% reduction at 15° tilt and a 74% reduction at 30° tilt. The dosimeter near the middle of the breast region measured dose reduction varying from 12% to 61% at tilt angles from 5° to 30°. The dosimeter in the inferior breast region experienced dose changes ranging from a 9% dose reduction to a 3% dose increase. As seen in Fig. **3**, which depicts a lateral scout and the 30° tilt direction, the superior region of the breast is expected to have the greatest dose reduction with gantry tilt due to being moved away from the irradiated beam.

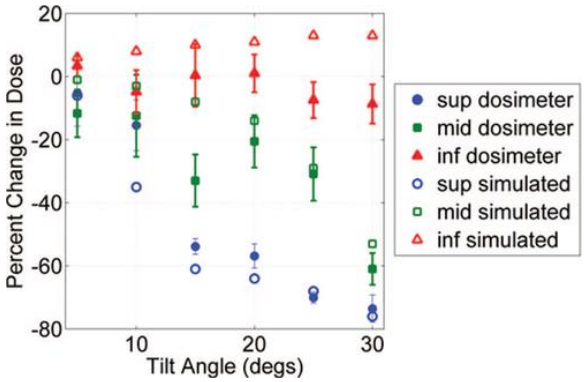

Figure 6 Relative change in dose for the three breast dosimeters as measured experimentally and as estimated through Monte Carlo simulations.

The relative breast dose estimated by the Monte Carlo simulations demonstrated similar trends and reasonable agreement with the experimental data. Differences in breast dose estimates between the simulations and experiments at a few tilt angles (e.g., the middle dosimeter at 15°) may be due to angular dependence of the MOSFET dosimeters or variations in surface dose with slice position.[22]

Figure **7** displays the percent change in noise standard deviation of the anthropomorphic phantom as measured experimentally and estimated through simulations. Both the experiments and simulations demonstrate decreased image noise with gantry tilt. The noise decrease is likely due to interpolation when the tilted slices are reformatted to the axial plane. The differences in noise reduction between the experiments and simulations may be due to differences in the reformatting algorithm.

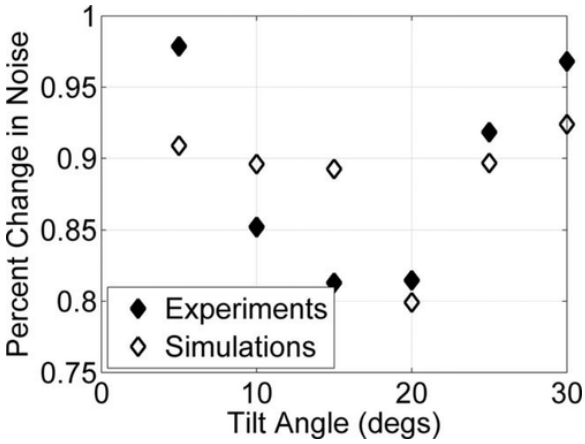

Figure 7 Relative change in noise in the anthropomorphic phantom as measured experimentally and as estimated through ray-tracing simulations.

III.B. Breast dose

Figure **8** plots the percent change in glandular breast dose at tilt angles of 0°–30° relative to the 0° tilt in 5° increments for all simulated phantoms, with each phantom denoted by a marker. Each voxelized phantom is denoted by the same marker for all plots in this paper. For comparison, the experimental dosimeter data are also plotted in Fig. **8**. Including all phantoms, the maximum %COV of the glandular breast doses estimated by simulation was 0.07% across the trials for a particular tilt angle.

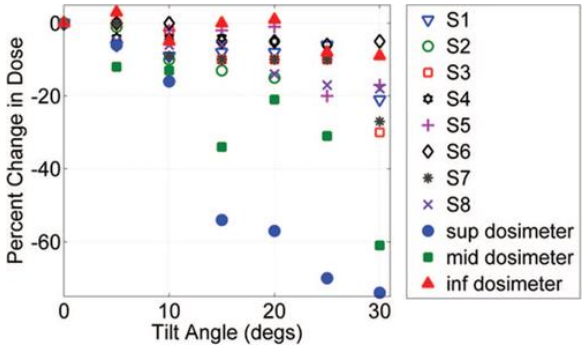

Figure 8 The percent change in glandular breast dose for the tilted acquisition relative to the 0° tilt for each voxelized phantom with respect to tilt angle. Each phantom is denoted by unique marker. The solid markers represent the change in dose in the experimental dosimeters.

As seen in Fig. **8**, tilting the gantry reduced the breast dose in all simulated phantoms, with generally greater dose reduction at increased gantry tilts. The percent reduction in breast dose varied across the eight phantom models at each tilt angle. For example, at 30° tilt, two of the phantoms demonstrated less than 10% dose reduction, two of the phantoms demonstrated ~20% dose reduction, and two phantoms demonstrated ~30% dose reduction. The dose reduction in the voxelized phantoms, which is calculated as dose to the whole breast tissue, was within the range of dose reduction measured in the inferior and midbreast dosimeters. The dosimeter placed in the superior region of the phantom breast demonstrated greater dose reduction than the voxelized phantoms. This result may occur because the simulation results estimate whole breast dose and the voxelized phantoms may have less breast tissue in the superior regions than the rigid breast phantoms.

III.C. Effects of tilted-gantry acquisition on noise standard deviation

Figure **9** displays sample reconstructed images of one voxelized phantom acquired at a 0° and 30° gantry tilt. Figure **10** plots the percent change in noise standard deviation at each tilt angle for all voxelized phantoms and

the experimental phantom. The noise standard deviation increased with tilt angle for all of the simulated voxelized phantoms, with the increase in noise standard deviation ranging from 2% to 50%. The experimental phantom demonstrated a reduction of noise standard deviation at all tilt angles ranging from 2% to 20% noise reduction. We hypothesized that the large difference in simulated noise performance between the anthropomorphic phantom (Fig. **7**) and the voxelized patient phantoms (Fig. **10**) was due to the fact that the experimental phantom did not include iodine in the blood pool, while the simulated phantoms modeled realistic iodine uptake. Tilted gantry acquisition increases the pathlength of rays through the heart, which attenuates more x rays, especially when the density of the material is high. To test this hypothesis, ray tracing simulations were performed for all voxelized phantoms with the blood modeled as water instead of diluted iodine. When the heart was modeled without iodine, as in the experimental phantom, the noise standard deviation decreased for seven of the eight phantoms (0%–50% noise reduction) for all tilt angles, and increased for one phantom for tilt angles greater 20°. Therefore, without iodine in the heart, the voxelized phantoms generally demonstrated reduced dose and noise, similar to the experimental phantom.

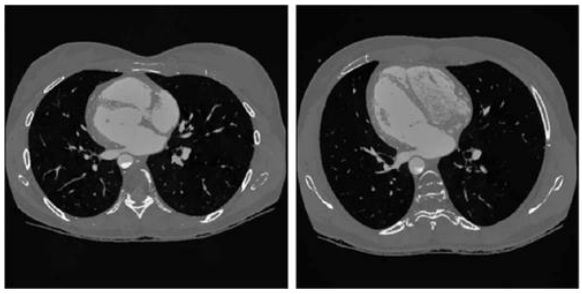

Figure 9 Reconstructed images of a voxelized phantom at 0° tilt (left) and 30° tilt (right).

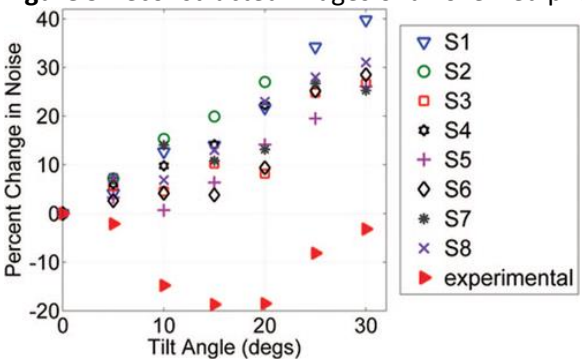

Figure 10 Percent change in noise standard deviation for the tilted acquisition relative to 0°. Each marker represents a specific phantom model.

Noise performance could be recovered by increasing the mAs, although this could increase dose to other tissues. We investigated whether there was a net reduction in breast dose for tilted-gantry acquisition if the noise standard deviation was required to be equal to the noise standard deviation at 0° tilt. To answer this question, the noise standard deviation ratio ($Noise_{tilt}/Noise_{0degrees}$) versus the dose ratio ($Dose_{tilt}/Dose_{0degrees}$) was plotted for each phantom and tilt angle (Fig. **11**). The plot also includes the curve representing the relationship that noise standard deviation varies inversely as the square root of dose. Points below this curve (shaded region in Fig. **11**) exhibit net breast dose reduction at equal standard deviation. Points above this curve are cases where the increase in noise standard deviation outweighs the dose reduction, leading to increased breast dose at noise standard deviation equal to the zero-tilt case. Thus, data points falling in the shaded gray region represent a net breast dose benefit, points in the white region represent a net breast dose detriment for the tilted-gantry acquisition, and points on the dividing line represent neither benefit nor detriment. As seen in Fig. **11**, none of

the voxelized phantoms demonstrated a net benefit in breast dose, with all but one of the phantoms demonstrating a net detriment in breast dose.

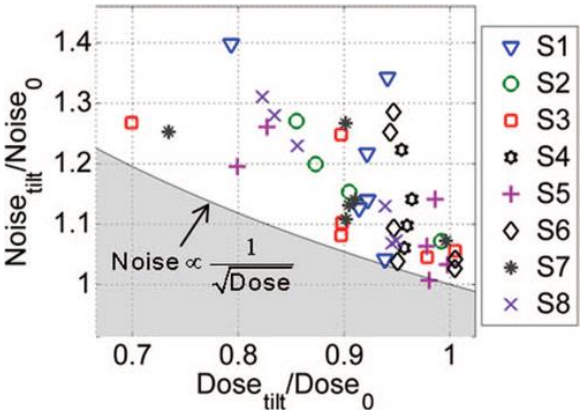

Figure 11 The ratio of noise standard deviation for tilted acquisitions relative to 0° tilt is plotted against the breast dose ratios for tilt angles between 5° and 30° in 5° increments. Also plotted is the relationship that noise standard deviation is inversely proportional to the square root of dose. The region above the curve represents points where the tilted gantry has a net detriment to dose.

Figure **12** plots the change in breast dose for all simulated phantoms estimated at noise standard deviation equivalent to the nontilted scan. The voxelized phantoms would have breast dose increases ranging from 0% to 70% with noise equivalent to nontilted scan.

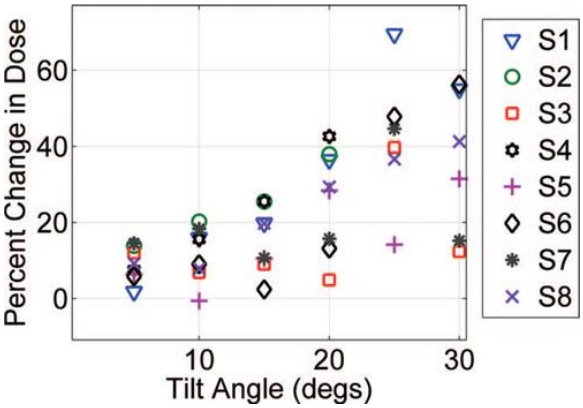

Figure 12 The estimated percent change in glandular breast dose when the reconstructed image noise standard deviation is equivalent to that of the nontilted scan. Each marker represents a unique simulated phantom.

IV. DISCUSSION

This study investigated imaging the heart region with gantry tilt angles between 0° and 30° through phantom experiments and simulation studies. This study was motivated by a previous study that demonstrated a reduction in irradiated breast volume with gantry tilt.[11] Both the experimental and simulation results in the current study demonstrated similar dose reduction values for the inferior, middle, and superior breast dosimeter locations. Validation of the ray-tracing simulation methods was limited by lack of knowledge about the reformatting algorithm used by the scanner software. Despite this limitation, both the experimental and simulated images estimated similar ranges of noise reduction with gantry tilt for the physical phantom. Based on this validation, the discrepancy between the results of the anthropomorphic phantom compared to the

voxelized phantoms appears to be due to limitations in the physical phantom, including rigid breast phantoms and lack of iodine in the blood pool.

The experimental and simulation results indicated reduced breast dose at all tilt angles, due to a decrease in irradiated breast tissue. However, tilted-gantry acquisition also increased the noise in all simulated voxelized phantoms, with the results suggesting that the noise increase was due to increased pathlength through the iodine-filled heart. The noise increase outweighed the breast dose reduction, such that the eight voxelized phantoms demonstrated a net increase in breast dose ranging from 0% to 70% with mAs increased to match the noise of the nontilted scan. One limitation of this study is the small number of patient phantoms (eight). Overall, the results of this pilot study indicate that tilted-gantry acquisition may not be effective for reducing breast dose while maintaining image quality.

A positioning device to move breast tissue in the superior direction has been shown to reduce breast dose.[23] Because the greatest dose reduction occurred in the superior breast region (Fig. **6**), combining a positioning device with gantry tilt may provide greater dose reductions and potentially a net breast dose benefit for all patients simulated in this study, although further studies are required to quantify these effects.

V. CONCLUSIONS

Tilting the gantry reduced breast dose by 0%–30%, with both experiments and simulations demonstrating generally greater dose reduction at increased tilt angles. However, increasing the gantry tilt also increased the noise standard deviation due to increased pathlengths through the iodine-filled heart, with noise increases ranging from 0% to 50%. Overall, the noise increase outweighed the dose reduction for the eight voxelized phantoms, suggesting that tilted gantry acquisition may not be beneficial for reducing breast dose while maintaining image quality.

ACKNOWLEDGMENTS

This work was funded in part by the Marion and Alvin Birnschein Foundation. Computing resources were provided by NSF Award No. OCI-0923037. The authors would like to thank Maureen Levenhagen RT(R), Medical College of Wisconsin, for data collection, and Jason Esveld, Marquette University, for assistance with segmentation.

REFERENCES

1 O. W. Linton and F. A. Mettler #1, " National conference on dose reduction in CT, with an emphasis on pediatric patients," *Am. J. Roentgenol.* **181**, 321– 329 (2003).10.2214/ajr.181.2.1810321

2 E. L. Nickoloff and P. O. Alderson, " Radiation exposures to patients from CT: Reality, public perception, and policy," *Am. J. Roentgenol.* **177**, 285– 287 (2001).10.2214/ajr.177.2.1770285

3 *2011 CT Market Outlook Report* (IMV Medical Information Division, Des Plaines, IL, 2011).

4 A. J. Einstein, M. J. Henzlova, and S. Rajagopalan, " Estimating risk of cancer associated with radiation exposure from 64-slice computed tomography coronary angiography," *JAMA, J. Am. Med. Assoc.* **298**, 317– 323 (2007).10.1001/jama.298.3.317

5 F. Faletra, I. D'Angeli, C. Klersy, M. Averaimo, J. Klimusina, E. Pasotti, G. Pedrazzini, M. Curti, C. Carraro, and R. DiLiberto, " Estimates of lifetime attributable risk of cancer after a single radiation exposure from 64-slice computed tomographic coronary angiography," *Heart* **96**, 927– 932 (2010).10.1136/hrt.2009.186973

6 E. Angel, N. Yaghmai, C. Jude, J. DeMarco, C. Cagnon, J. Goldin, C. McCollough, A. Primak, D. Cody, and D. Stevens, " Dose to radiosensitive organs during routine chest CT: Effects of tube current modulation," *Am. J. Roentgenol.* **193**, 1340– 1345 (2009).10.2214/AJR.09.2886

7 L. M. Hurwitz, T. T. Yoshizumi, P. C. Goodman, R. C. Nelson, G. Toncheva, G. B. Nguyen, C. Lowry, and C. Anderson-Evans, " Radiation dose savings for adult pulmonary embolus 64-MDCT using bismuth breast shields, lower peak kilovoltage, and automatic tube current modulation," *Am. J. Roentgenol.* **192**, 244– 253 (2009).10.2214/AJR.08.1066
8 S. Leschka, C. H. Kim, S. Baumueller, P. Stolzmann, H. Scheffel, B. Marincek, and H. Alkadhi, " Scan length adjustment of CT coronary angiography using the calcium scoring scan: Effect on radiation dose," *Am. J. Roentgenol.* **194**, W272– W277 (2010).10.2214/AJR.09.2970
9 G. L. Raff, K. M. Chinnaiyan, D. A. Share, T. Y. Goraya, E. A. Kazerooni, M. Moscucci, R. E. Gentry, and A. Abidov, " Radiation dose from cardiac computed tomography before and after implementation of radiation dose-reduction techniques," *JAMA, J. Am. Med. Assoc.* **301**, 2340– 2348 (2009).10.1001/jama.2009.814
10 C. McCollough, D. Cody, S. Edyvean, R. Geise, B. Gould, N. Keat, W. Huda, P. Judy, W. Kalender, and M. McNitt-Gray, " The measurement, reporting, and management of radiation dose in CT," AAPM TG 23 Report No. 96, 2008.
11 E. J. Halpern, K. M. Takakuwa, E. L. Gingold, and D. J. Halpern, " A novel approach to reduce breast radiation exposure with coronary CTA: Angled axial image acquisition," *Acad. Radiol.* **16**, 951– 956 (2009).10.1016/j.acra.2009.02.009
12 J. Geleijns, M. S. Artells, W. J. H. Veldkamp, M. L. Tortosa, and A. C. Cantera, " Quantitative assessment of selective in-plane shielding of tissues in computed tomography through evaluation of absorbed dose and image quality," *Eur. Radiol.* **16**, 2334– 2340 (2006).10.1007/s00330-006-0217-2
13 C. Hohl, J. E. Wildberger, C. Suss, C. Thomas, G. Muhlenbruch, T. Schmidt, D. Honnef, R. W. Gunther, and A. H. Mahnken, " Radiation dose reduction to breast and thyroid during MDCT: Effectiveness of an in-plane bismuth shield," *Acta Radiol.* **47**, 562– 567 (2006).10.1080/02841850600702150
14 K. D. Hopper, S. H. King, M. E. Lobell, T. R. TenHave, and J. S. Weaver, " The breast: In-plane x-ray protection during diagnostic thoracic CT–shielding with bismuth radioprotective garments," *Radiology* **205**, 853– 858 (1997).
15 J. Wang, X. Duan, J. A. Christner, S. Leng, L. Yu, and C. H. McCollough, " Radiation dose reduction to the breast in thoracic CT: Comparison of bismuth shielding, organ-based tube current modulation, and use of a globally decreased tube current," *Med. Phys.* **38**, 6084– 6092 (2011).10.1118/1.3651489
16 S. Vollmar and W. Kalender, " Reduction of dose to the female breast in thoracic CT: A comparison of standard-protocol, bismuth-shielded, partial and tube-current-modulated CT examinations," *Eur. Radiol.* **18**, 1674– 1682 (2008).10.1007/s00330-008-0934-9
17 A. J. Reilly and J. Addison, " Evaluation of a nonenhanced helical CT protocol for detecting ureteric stones," *Radiology* **221**, 558– 559 (2001).10.1148/radiol.2212010488
18 K. Cranley, B. Gilmore, G. Fogarty, and L. Desponds, " IPEM Report 78: Catalogue of diagnostic x-ray spectra and other data," CD-Rom edition, 1997.
19 S. E. McKenney, A. Nosratieh, D. Gelskey, K. Yang, S.-Y. Huang, L. Chen, and J. M. Boone, " Experimental validation of a method characterizing bow tie filters in CT scanners using a real-time dose probe," *Med. Phys.* **38**, 1406– 1415 (2011).10.1118/1.3551990
20 S. Agostinelli, J. Allison, K. Amako, J. Apostolakis, H. Araujo, P. Arce, M. Asai, D. Axen, S. Banerjee, and G. Barrand, " GEANT4—A simulation toolkit," *Nucl. Instrum. Methods Phys. Res. A* **506**, 250– 303 (2003).10.1016/S0168-9002(03)01368-8
21 ICRP, " Adult Reference Computational Phantoms. ICRP Publication 110," *Ann. ICRP* 39 (2009).
22 D. Zhang, A. S. Savandi, J. J. Demarco, C. H. Cagnon, E. Angel, A. C. Turner, D. D. Cody, D. M. Stevens, A. N. Primak, and C. H. McCollough, " Variability of surface and center position radiation dose in MDCT: Monte Carlo simulations using CTDI and anthropomorphic phantoms," *Med. Phys.* **36**, 1025– 1038 (2009).10.1118/1.3078053
23 S. J. Foley, M. F. McEntee, S. Achenbach, P. C. Brennan, L. S. Rainford, and J. D. Dodd, " Breast surface radiation dose during coronary CT angiography: Reduction by breast displacement and lead shielding," *Am. J. Roentgenol.* **197**, 367– 373 (2011).10.2214/AJR.10.4569